Assessment of small-strain modulus through wave velocity measurement with dynamic penetrometer Panda 3®

C. F. Oliveira
Pascal Institute, Clermont-Auvergne University, Clermont-Ferrand, France, caroline.forestti_oliveira@etu.uca.fr

M. A. Benz-Navarrete[1], Q. A. Tran[2]
Sol-Solution Géotechnique Réseaux, Riom, France, mnavarrete@sol-solution.com[1], qatran@sol-solution.com[2]

Pierre Breul[3], Bastien Chevalier[4], Claude Bacconnet[5]
Pascal Institute, Clermont-Auvergne University, Clermont-Ferrand, France, pierre.breul@uca.fr[3], bastien.chevalier@uca.fr[4], claude.bacconnet@univ-bpclermont.fr[5]

ABSTRACT: Field determination of small-strain modulus (E_0) and compressional wave velocity (c_p) is a major issue. Even though many techniques allow determining these parameters, most of them are not able to provide precise and reliable data at low-cost. Moreover, most of these techniques do not allow to assess a soil strength parameter. Panda 3® is a dynamic penetrometer for shallow soil characterization. The device's principle consists to measure wave propagation within the rod to each blow during driving. Force and acceleration measurements combined with signal analyses allow the obtain stress and velocity generate by the impacts. An approach based on the shock theory is proposed to determine c_p and E_0 from shock related equations. This paper presents the principle and the theoretical background applied. Additionally, shock relationships provide an estimating of soil axial stress-strain response during each shock. The results from a series of test carried out in calibration chamber on two sands at different densities, moisture contents and confining stresses are presented. These results are compared to those reported in the literature.

Keywords: *in situ* testing; Panda 3® penetration test; shock test; small-strain modulus; wave velocity.

1. Introduction

Soil's failure and deformation parameters are key to geotechnical design. These parameters are determined by *in situ* and/or laboratory tests. Dynamic penetration tests are widely known as an easy and low-cost technique routinely applied to assess soil strength parameters. Nevertheless, this technique *a priori* does not allow to evaluate soil's deformability once the penetration is mostly a high-strain associated phenomenon.

Soil's deformability modulus is highly dependent upon the strain level [1] [2]. Soil's small-strain parameters are mainly determined whether by wave velocity tests or resonance tests [3]. In laboratory most common techniques are piezoceramic elements and resonant column test, and *in situ* by seismic test such as surface wave methods (*e.g.* MASW, SASW) or borehole tests (*e.g.* cross-hole, down-hole).

Surface wave testing is appealing for its non-destructive and non-invasive nature and also because they are able to sample a representative volume of the ground even in difficult materials (fractured rocks or gravelly deposits). However, often these techniques employs inverse analysis which can produce some incertitude. On the other hand, borehole tests are appreciated due to its reliability and precision, but they are more expensive and time-consuming.

Moreover, in general, none of these methods (surface and borehole tests) provide soil shear strength parameters other than by means of correlation. Thus, in geotechnical design, often these tests should be associated to other techniques who are able to evaluate soil failure behaviour such as SPT and CPT.

To obtain parameters at two opposite ends of the strain spectrum (*i.e.* in low-amplitude such as c_p[1], E_0 and in large-strain behaviour, such as strength parameters), seismic cone penetration test or seismic dilatometer can be employed [4] [5]. Although, these techniques are less common and a more extensive than a dynamic penetrometer test.

The main objective of this study is to propose a methodology to determine soil small-strain modulus through a dynamic penetrometer and thus to provide simultaneously soil strengh and a soil deformability parameter.

Laboratory test were carried out in order to evaluate the method. Experimental program consists in a series of penetrometer test carried out in a calibration chamber on two sandy soils. Specimens were reconstituted by wet compacted with moisture contents around 3% in different densities (relative density of 20% and 40%). Samples were confined under different stresses (25kPa and 50kPa) by means of an overload.

[1] The letter c indicates wave velocity instead of the classical notation (v) to avoid any misunderstading between this parameter and particle velocity (which will be later on indicated by the letter v).

2. Soil small-strain modulus

Soil's deformability modulus is highly dependent upon the strain level. The soil's modulus determined by traditional laboratory test such as classical external sensor triaxial test are unable to evaluate soil's deformability under 10^{-3} level. As a result, modulus determined by triaxial or oedometric test underestimate soil's maximum modulus. [1] observed maximum modulus that were five times bigger than results from careful laboratory tests.

Initially, these gap were attributed to sampling effects. Later on, with development of more precise laboratory measurement, it became clear that the gap was due to soil's deformability degradation though strain spectrum [1]. Many studies shown the importance of a reliable estimation of soils small-strain deformation to the various geotechnical application [1] [2]. In most of the cases, E_0 is obtained from wave velocity measurements whether *in situ* or in laboratory. According to fundamental dynamic principle, under linear elastic isotropic state, small-strain modulus is related to wave velocity (c_p) and soil mass density (ρ) by Eq (1).

$$E_0 = c_p^2 \rho \quad (1)$$

Often in geotechnical practice, soil mass density is merely estimated as a given average value (unit weight of γ=18 kN/m^3). In fact, unit weight of natural soils varies from around 10kN/m^3 to 21kN/m^3. In clean sands, unit weight are well-related to tip resistance [5]. In fact, to certain moisture content, there is a one-to-one relationship between these two parameters. They are related by a logaritmic law. A data basis have been established to A, B and C to different soil types allowing to estimate soil's density [6] [7].

$$\gamma_d = A(w) + Bln(q_d) + C \quad (2)$$

In this precise study, soil unit weight is directly determined. In case of a conventional *in situ* campaign, once the type of soil is known, Eq. (2) can provide a unit weight estimation from penetrometer results. Figure 4 illustrates the whole methodology proposed to determine soil's small-strain modulus through Panda 3® test.

It's worth noting that small-strain modulus depends on a number of parameters (grain size distribution, soil's history, plasticity, confining stress, saturation). Different studies have shown that in the case of sands, the small-strain modulus is strongly influenced by the void ratio (or relative density) and the effective confining pressure [8] [9] Consequently, some of empirical relationships between small-strain modulus, void ratio and confining pressure stress have been proposed from laboratory results. The empirical model proposed by Biarez & Hicher [10] is accepted as a good approximation for geomaterials in isotropic conditions (Eq. (3)).

$$E_0 = \frac{450}{e} p'^{0.5} \quad (3)$$

3. Shock test in soils

High-velocity penetration of solids is a complex topic of impact dynamics mostly because it involves a wide variety of their physical-mechanical properties. Even though shock test are not traditionally applied to characterize soil parameter, they can be a useful mean to evaluate soil behaviour at high deformation rates and high stress. These theories were applied to sands by using Split Hopkinson Pressure Bar (SHPB) or Kolsky bar apparatus. Although, the characterisation of sand by these means is more complex than for conventional materials (e.g. metals) as longitudinal waves in granular media are influenced by many parameters such as grain size distribution, moisture content and degree of compaction. Some authors have successfully determined the longitudinal wave velocity by Kolsky bar test [11].

In shock tests, deformation in the shock wave front is assumed to occur mainly in one-dimensional, thus the test can be assimilate to a confined compression test. Because the shock generates a high stress increase, soil shows no resistance to propagation wave, behaving similar to a fluid. Application of fluid dynamic shock equations is then accepted. These equations result from conservation of mass, momentum and energy during the shock. They relate stress σ, particle velocity v and wave velocity D to media parameters (bulk initial density ρ_0 and elastic modulus E) [12] [11].

Particle velocity v and stress σ are related by the product of ρ_0 and wave velocity D, *i.e.* by mechanical impedance ($Z = \rho_0 D$) (Eq. (4)). In the elastic domain, wave velocity is constant and D = c, where c is sonic velocity. Beyond a certain particle velocity, wave velocity varies with particle velocity. This relation is in most of cases described by an increasing linear relation, but can also be expressed by a quadratic model as it depends on shock conditions and energy-absorption (Eq. (4)) [13] [14] [15]. As a result, in elastic domain, the relation between particle velocity and stress is a linear relationship. Beyond the elastic domain, this relationship is usually parabolic. These two patterns are expressed by Eq. (4) where A and B are coefficients that depend only on the downstream media. The relationship between particle velocity and stress is often referred as shock polar curve [16].

$$\sigma_{xx} = D\,\rho_0 v \begin{cases} \sigma_{xx} = c\,\rho_0 v \\ (Elastic\ domain, D = c) \\ \sigma_{xx} = (A + Bv)\,\rho_0 v \\ (Non - elastic\ domain) \end{cases} \quad (4)$$

Considering mass conservation during wave propagation, [13] has shown that strain in the direction of wave propagation can be expressed by particle velocity v and wave velocity D (Eq. (5).

$$\varepsilon_{xx} = v/D \quad (5)$$

Aussedat (1970) introduces the application of state equations to dynamic penetrometer test. He proposes a number of simplifications and develops a laboratory penetrometer (Figure 1a). Figure 1b and c presents experimental results to a series of impacts on sandy soils [13]. Low and high stress shocks were then performed in a clayey soil (Eybens clay) tested in laboratory and in situ. He precises that the application of state equations to penetrometer test involves the following hypothesis and considerations:

- The contact between soil and tip during wave transmission is assumed to be plane and perpendicular;

- Damping is negligible while wave propagates within the rod;
- Even if the rod encounteres simultaneously radial (ε_{rr}) and longitudinal strain (ε_{zz}) during driving, the mass conservation is still verified in longitudinal direction. Longitudinal stress is directly measured on the rod hence the relation $\sigma_{zz} = \gamma c\, v$ can still be applied.

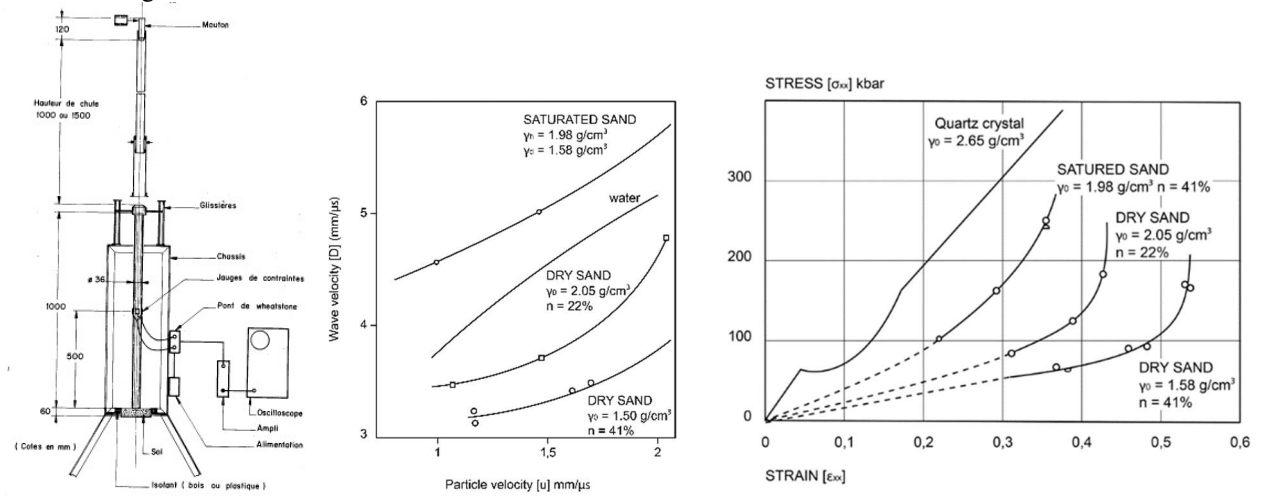

(a) (b) (c)

Figure 1. (a) Laboratory dynamic penetrometer developed by Aussedat [13], (b) Wave velocity D and particle velocity v relationship (adapted from [13]) and (c) Stress and strain relationship obtained for sandy soils (adapted from [13]).

- During the time of whole event (propagation of incident and reflected longitudinal wave) the soil radial strain is negligible. Considering wave propagation c in steel of around 5200m/s and a rod length L of 1m, the pulse transit all the way. down and back takes around 350µs (dt = 2L/c). Within this time interval, the rupture bulb is not yet created and soil strain occurs mainly in vertical direction close to the rod's tip. [13] have determined wave velocity and strain for a series of impacts by soils shock polar curve construction

Table 1. Wave velocity and strain level determined by Aussedat's tests in clayey soil [13]

σ_0 (kPa)	σ_0 (kPa)	v (m/s)	σ_0 (kPa)	D (m/s)	ε (10^{-3})
4400	3500	0.56	900	780	0.7
5200	4400	0.68	800	570	1.2
7000	5800	0.90	1200	650	1.4

Thus, [13] showed that the shock principle can be applied to penetrometer test. Nonetheless, technical issues (number and precision of sensors) and wave overlay limit these tests to research context.

4. Panda 3® lightweight penetrometer

Panda 3® is a lightweight dynamic penetrometer. The device is driven by hand-hammer blows on the anvil. The operator is able to adapt the applied energy to stiffness of soil [17] [18].

The sensors placed close the anvil measure strain *ε(x,t)* and the acceleration *a(x,t)* inducted by the compressional wave propagation during penetrometer driving. The compressional wave is created by each impact and propagates throughout the rods and back. A displacement sensor in the microprocessor device is placed at ground level and connected to the anvil. It allows record simultaneously the cone penetration displacement throughout the test. The Human Computer Interaction (HCI) device allows configuration of test details and display of results all along test execution.

During the test the hammer shock generates a compressional wave which propagates within the rod at the velocity c (~5200m/s for steel) towards the cone. Once this wave reaches the soil, part of it is reflected and the rest is transmitted to the soil. The energy transmitted to the soil is responsible for penetration observed. The reflected compressional wave get to the anvil and then back to the bottom. Multiple reflections occur and the phenomenon becomes cyclical as the energy decreases.

Rods are assumed elastic and with constant section A. External forces along the rods such as skin friction are considered insignificant. Hence, the compressional wave propagation can be described by Alembert's equation known as wave equation (Eq. (6)).

$$\frac{\partial^2(x,t)}{\partial t^2} = c^2 \frac{\partial^2 u(t,x)}{\partial x^2} \tag{6}$$

A general solution to Eq. (6) corresponds to the overlay of downward $u_f(x - ct)$ and upward $u_g(x + ct)$ waves, where u_f and u_g are arbitrary respectively functions (Eq. (7)).

$$u(x,t) = u_f(x - ct) + u_g(x + ct) \tag{7}$$

By assessing u_f and u_g at a point x_A in the rods its possible to determine the corresponding stress σ(x,t), strain ε(x,t), velocity v(x,t) and displacement u(x,t). For a plane wave and a single mode of propagation, strain, stress, velocity and displacement can be expressed in terms of the Fourier transforms (Eq.(8)-(11)).

$$\tilde{\varepsilon}(x,\omega) = A(\omega)e^{-i\xi(\omega)x} + B(\omega)e^{i\xi(\omega)x} \tag{8}$$

$$\tilde{\sigma}(x,\omega) = E^*(\omega)\left[A(\omega)e^{-i\xi(\omega)x} + B(\omega)e^{i\xi(\omega)x}\right] \tag{9}$$

$$\tilde{v}(x,\omega) = -\frac{\omega}{\xi(\omega)}\left[A(\omega)e^{-i\xi(\omega)x} - B(\omega)e^{i\xi(\omega)x}\right] \quad (10)$$

$$\tilde{u}(x,\omega) = \frac{i}{\xi(\omega)}\left[A(\omega)e^{-i\xi(\omega)x} - B(\omega)e^{i\xi(\omega)x}\right] \quad (11)$$

Next, upward and downward waves are separated. There are different methods of wave separation and reconstruction. Their application depends of types and quantity of sensors employed as well as initial and boundary conditions [19] [20] [21]. In the Panda 3® the employed method is based on a single point measurement on the rod which is placed close to the anvil [20]. In this point, strain and acceleration are recorded. Velocity is obtained by integration of acceleration data. In the single point measurement x_A, the downward $\varepsilon_f(x\text{-}ct)$ and upward strain $\varepsilon_g(x+ct)$ waves are separated in time domain from $\varepsilon_A(t)$ and $v_A(t)$ recorded signals.

$$\varepsilon_f(x-ct) = \frac{1}{2}[\varepsilon_A(t)] - \frac{1}{2c}[v_A(t)] \quad (12)$$

$$\varepsilon_g(x+ct) = \frac{1}{2}[\varepsilon_A(t)] + \frac{1}{2c}[v_A(t)] \quad (13)$$

Once $\varepsilon_f(x\text{-}ct)$ and $\varepsilon_g(x+ct)$ are separated at the specific point A, stress, velocity and displacement are reconstructed at penetrometer's tip located at a distance $(x_J - x_A)$ below the measurement point A.

Assuming no variations of external forces and mechanical impedance constant along the rods, the iterative method proposed by [22] is used to rebuild stress $\sigma_n(t)$ a velocity $v_n(t)$ for each x_n section along the rods, especially when mechanical impedance changes occurs (Eq. (14)).

$$\sigma_n(t) = 1/2\left[\sigma_{n-1}\left(t+\Delta t_{n-(n-1)}\right) + \sigma_{n-1}\left(t-\Delta t_{n-(n-1)}\right)\right] \ldots + Z_n/2\left[v_{n-1}(t+\Delta t_{n-(n-1)} - v_{n-1}(t+\Delta t_{n-(n-1)})\right] \quad (14)$$

$$v_n(t) = 1/2\left[v_{n-1}\left(t+\Delta t_{n-(n-1)}\right) + v_{n-1}\left(t-\Delta t_{n-(n-1)}\right)\right] \ldots + 1/2\,Z_n[\sigma_{n-1}(t+\Delta t_{n-(n-1)} - \sigma_{n-1}(t+\Delta t_{n-(n-1)})] \quad (15)$$

Being $\Delta t_{n-(n-1)} = (x_{n-1} - x_n)/c$ and $\Delta Z_n = \left(\frac{E_n}{c}\right)$. With Z_n, E_n and c are respectively mechanical impedance, elastic modulus and wave velocity measured at the section n. According to this technique, if the geometry and distance between impedance changes planes are known, the stress and velocity at the lower extremity n can be calculated from previous measurement n-1 point where stress and velocity were known (Figure 2).

In the case of current penetrometer device, where rods are elastic and homogenous, as well as there are no impedance changes at the connectors sections and no external skin forces, the only impedance change take place at tip/rod screwing section. The tip signal rebuilding is done by two iteration of Eq. (14), as follow:

- In the first iteration, stress $\sigma_C(t)$ and velocity $v_C(t)$ signal for section C (noted n) in calculated (Figure 2) from the signal $\sigma_A(t)$ and $v_A(t)$ recorded in the measurement section A (or n-1) by mean of Eq.(14).
- In the second iteration, stress $\sigma_t(t)$ and velocity $v_t(t)$ signals for section J (Figure 2**)** are calculated from stress and velocity records that has been calculated previously for section C. In Eq. (14), J and C signal are noted respectively as n and n-1 section.

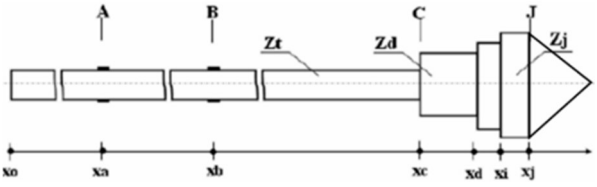

Figure 2. Scheme of penetrometer showing different sections A (measurement point) and B, C and J (points of wave reconstruction) (adapted from [22]).

Once the stress $\sigma_t(t)$ and velocity $v_t(t)$ records are calculated for the penetrometer tip, strain $\varepsilon t(t)$ and strength $F_t(t)$ are calculated by mean of elasticity relationships. Displacement $u_t(t)$ is calculed thought numerical integration. Next, assuming stresses and displacements equal in cone/soil interface during the cone penetration, cone stress-penetration curve is determined.

Determination of wave velocity through Panda 3®

Panda 3® test allows to measure stress and particle velocity evolution in the rod during the shock. Once the incident and reflected stress wave are determined by wave separation method, transmitted wave (σ_t and v_t) is deduced. Transmitted stress wave allows to build soil's shock polar curve.

[17] was the first to apply this approach to Panda 3® test. He carried out tests with different materials. Shock polar curve of testing materials attest the sensitivity and repeatability of this method. In this approach, wave velocity of soil c_s is determined with the pic stress (σ_f and σ_g) and particle velocity (v_f and v_g) data of incident and reflected waves (Eq.(16)).

$$\sigma_f - \sigma_g = \rho_s\, c_s(v_f + v_g) \quad (16)$$

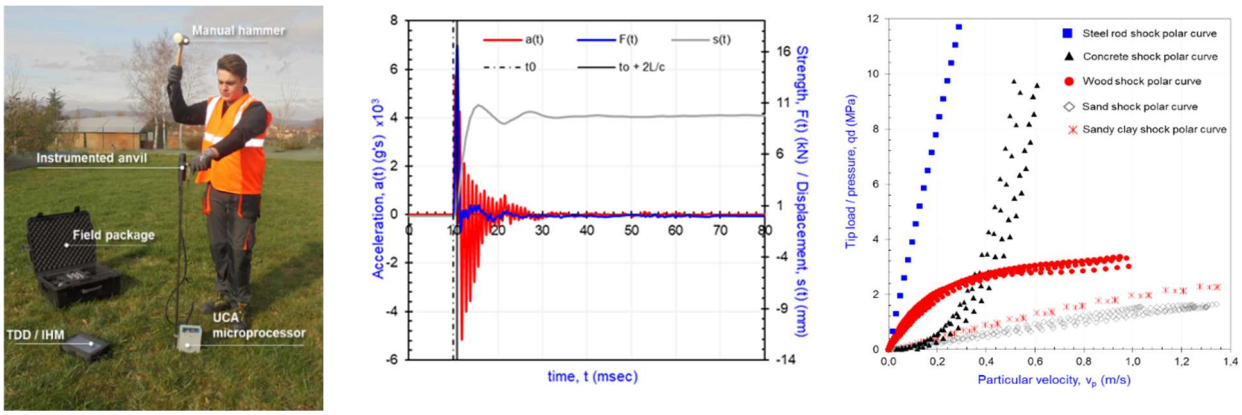

(a) (b) (c)

Figure 3. (a) Dynamic penetrometer Panda 3® apparatus, (b) Example of Panda 3® raw data (force, acceleration and displacement signals) recorded for one single blow [17] and (c) Experimental shock polar curve obtained for different materials (steel rods, concrete, wood and sand). [17]

The application of Eq. (16) is justified by the short time interval of the whole event (pulse transit down and up the rod, *i.e.* 320µs). [17] laboratory test results show a good agreement to testing materials velocity wave (Table 1)

Table 1. Wave velocity of laboratory test results [17]

Material	$\overline{c_p} \pm \sigma$ **(m/s)**
Concrete	3768 ± 403,6
Wood	5250 ± 244,9
Allier sand(γ ~16,5kN/m³)	789 ± 82,6
Allier sand(γ ~14,5kN/m³)	432 ± 112,6

Wave velocity tests were carried out in clay-marl formation in France [23]. Surface technique MASW and Panda 3® tests were executed in adjacent spots. Results show good agreement between both methods. Shear wave velocity (c_s) was estimed by c_p results and Poisson's ratio ν (Eq. (17)) and compared to MASW profiles.

$$c_s = \sqrt{\frac{1-2\nu}{2(1-\nu)}}c_p \qquad (17)$$

Shock polar curve from single blow data fitting

During Panda 3® test, velocity and stress are measured almost continuously (frequency 50kHz to 100kHz) for each block. The approach introduced by [17] provides a fair determination of compression wave velocity [23], nevertheless Panda 3® allows to evaluate stress and particle velocity increase continuously during one single shock. Hence, it is possible to analyse soil response gradually. In fact, Aussedat suggests that stress and particle velocity increase produced by wave propagation can be exploit in multi-steps. Using this approach, it is possible to perceive an impact as a series of shocks of a growing stress. This would allow to observe show soil's behaviour change and to limit wave velocity determination to the linear domain. Beyond this zone, wave velocity is expressed as a function of particle velocity so it would longer correspond to sonic wave velocity.

In fact, in laboratory shock tests such as oedometric shock test, boundary conditions are well-defined and specimen size is small enough to more easily meet equation state conditions. Nevertheless, some experimental results suggest a highly repeatibility of shock polar curve. This fact motivate us to evaluate the application of a new approach to some zones of the specimen where this phenomenon has been encountered.

Experimental program were carried out to evaluate the method. It consists in a series of penetrometer test on two sandy soils carried out in a calibration chamber under different conditions.

5. Experimental program

Tested materials

The soils tested were Hostun sand (HS) and Fontainebleau sand (FS). These are two siliceous sands with angular grains. These soils were selected because of the large laboratory test results reported not only for conventional tests but especially for small-strain parameters [24] [25]. The soils characterisation results as well as the literature data are summarised in Table 2.

Table 2. Selected sands characteristics [25] [26] [27]

Soil	Present study		Reported in literature*			
	d_{50} (mm)	C_u	e_{min}	e_{max}	c_p (m/s)	E_0 (MPa)
HS	0.38	1.54	0.60	0.93	119.5 - 412.1	20.4 - 252.5
FS	0.23	1.72	0.62	0.96	139.6 – 267.2	28.7 - 113.5

*e values from [24]; v_p and E_0 values from [25] [26] [27].

Sample preparation and test procedure

All samples were prepared by wet dynamic compaction. Water were added so all sample would have same moisture content (2-5%). Next, homogenized soil was dynamically compacted inside the chamber in layers by using a rammer. Constant compaction energy was applied to each layer. Soil's density was controlled throughout the compaction by measuring mass and volume after each layer compaction. Additionally, homogeneity was later on attested by Panda 3® penetrogram results (Figure 4).

Depending on the vertical and horizontal displacements (δ_v and δ_h) and stresses (σ_v and σ_h) in the

calibration chamber during penetration, boundary condition (BC) can be classified in four types: BC1 ($\sigma_v = \sigma_h = 0$), BC2 ($\delta_v = \delta_h = 0$), BC3 ($\delta_v = 0$ and σ_v = constant), or BC4 ($\delta_v = 0$ and σ_h = constant) [28]. This nomenclature is usual when dealing with calibration chamber boundary conditions. In this study, boundary conditions correspond to the BC3 type *i.e.* vertical stress is kept constant and no radial displacement is allowed.

The vertical stress is added by means of an overload (25kPa and 50kPa). Perforated metallic plates are placed on the chamber surface imposing a constant vertical stress. During the test a PVC tube placed around the rod prevent lateral friction between rod and the soil. A Panda 3® test was effectued at the axis of chamber. After, the test soil samples are collected to moisture content determination in oven.

Upward and downward waves are obtained through force and acceleration measurements and separation and reconstruction wave method as described previously. Stress and particle velocity of the transmitted wave is then deduced incident and reflected wave signals within velocity increasing.

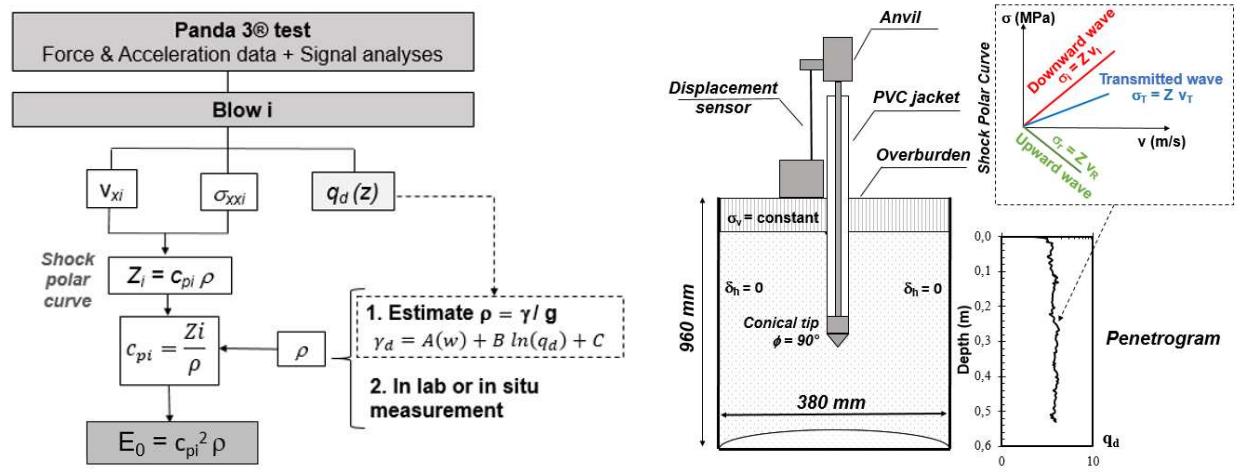

(a) (b)

v_{xi} = particle velocity of the blow i, σ_{xxi} = stress of the blow i, q_d = tip resistance, Z_i = mechanical impedance, c_{pi} = compressional wave, ρ = soil mass density, A and B = empirical coefficients, γ = soil unit weight, g = gravitational acceleration, E_0 = small-strain modulus

Figure 4. (a) Schema to determine small-strain modulus from Panda 3® test for a blow i and (b) Experimental set-up, penetrogram and velocity wave determination method applied to each blow

6. Results and discussion

Penetrograms of the eight tested specimens are presented in Figure 6 as well as tip resistance values. Specimen's characteristics as well as wave velocity and small-strain modulus are presented summarized in Table 3. Wave velocities were obtained from the average shock polar curve of a series of five consecutive impacts Average mechanical impedance is determined from linear regression of linear assumed zone, and then wave velocity is obtained from mass density ($Z=c\rho$). Figure 5a illustrates the method. Next, small-strain modulus is determined from wave velocity and mass density by Eq. (1).

Table 3. Experimental results to the tested sands

Sample	w (%)	e	DR (%)	σ_v (kPa)	Z (MPa/(m/s))	c_p (m/s)	E_0 (MPa)
HS1	2.5	0.94	25	25	0.330 ± 0.06	236	78
HS2	2.9	0.88	41	25	0.357 ± 0.03	253	93
HS3	2.7	0.95	21	50	0.416 ± 0.13	270	96
HS4	2.2	0.88	42	50	0.521 ± 0.06	361	188
FS1	4.5	0.85	39	25	0.324 ± 0.04	213	69
FS2	4.4	0.77	56	25	0.360 ± 0.02	226	81
FS3	4.6	0.87	16	50	0.288 ± 0.03	201	58
FS4	4.5	0.97	55	50	0,439 ±0.06	276	121

HS = Hostun sand, FS = Fontainebleau sand, w = moisture content, DR = relative density, σ_v = overburden applied.

In general, the results to small-strain modulus obtained are of the same order of literature data results (Table 2). It is important to notice that sand key factors (relative density and overburden pressure) are not identical, so a direct comparison is not possible.

Once, test conditions are not the same, results of this study and of literature data are compared to Hicher & Biarez (1994) empirical model. Figure 5c show that variation of the results of this study are comparable to variation of literature data from laboratory tests deduced from other techniques (laboratory cross-hole and piezoceramic elements tests).

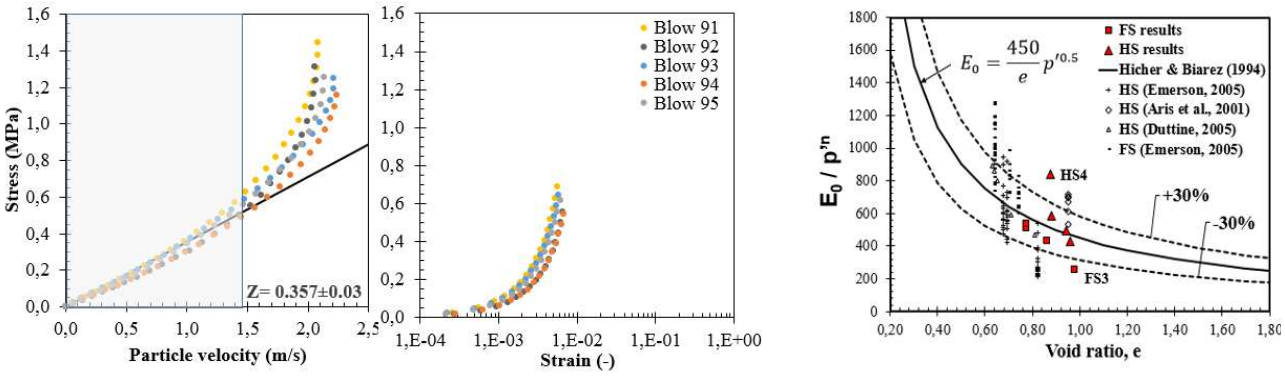

(a) (b) (c)

Figure 5. Example of results (a) Shock polar curve to a series of five consecutive blows of HS2 specimen (DR=41%, σ_v =25kPa) and mechanical impedance deduced to the linear assumed zone (grey zone) (b) Stress and strain relationship in linear assumed zone expressed in log scale (c) Experimental results and literature data evaluation by Hicher et Biarez (1994) model.

Shock tests are often applied to estimate stress-strain material behaviour. In fact, in plate impact experiments, uniaxial stress induced by impact in direction of shock propagation is much higher than deviatory effects. So, in weak materials such as sands, the stress σ_x in the direction of wave propagation [25].

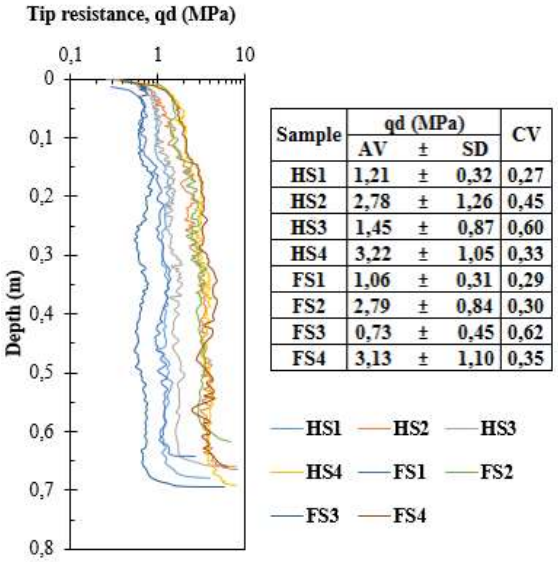

Sample	qd (MPa) AV	±	SD	CV
HS1	1,21	±	0,32	0,27
HS2	2,78	±	1,26	0,45
HS3	1,45	±	0,87	0,60
HS4	3,22	±	1,05	0,33
FS1	1,06	±	0,31	0,29
FS2	2,79	±	0,84	0,30
FS3	0,73	±	0,45	0,62
FS4	3,13	±	1,10	0,35

Figure 6. Penetrograms of the specimens and tip resistance results

It can be also assumed that for this short time interval, stress-velocity increase and strain are mostly uniaxial. If we analyse the linear assumed domain the application of axial strain ε_{xx} = v/c, with c constant to this zone. Evolution of the axial strain is evaluated in function of stress increase to this zone. Figure 5(b) illustrate the application of approach to specimen HS2. Results suggests a strain interval associated to the impact from 10^{-4} to 10^{-2} strain.

7. Conclusion

Being able to assess soil strength and deformability behaviour through a single rapid *in situ* technique would provide economical and technical gains. It would allow to evaluate soil under field conditions and to optimize experimental campaigns.

A methodology is presented to determine small-strain parameter (c_p and E_0) through a rapid and low-cost *in situ* testing technique: the Panda 3® penetrometer test. To illustrate its application, wave velocity is determined to a series of consecutive impacts of eight specimens. Two sands were tested in a calibration chamber in different states (DR and confining pressure). Results show good agreement with the literature data. A larger experimental campaign must be carried out in order to validate the methodology to more representative number of impacts and to other soils under different conditions.

The present work is part of a research project which aims to determine soil's deformation (by modulus degradation curve estimation) and shear strength parameters (cohesion and friction angle) by lightweight penetrometer test.

References

[1] J. B. Burland, "Ninth Laurits Bjerrum Memorial Lecture:" Small is beautiful"—the stiffness of soils at small strains," vol. 26, no. 4, pp. 499-516, 1989.

[2] R. J. Jardine, Some observations on the kinematic nature of soil stiffness. Soils and foundations, vol. 32, n° 12, pp. 111-124, 1992.

[3] C. Dano and P. Y. Hicher, "Mesure du module de cisaillement de différents matériaux par la technique des bender elements," in In PARAM2002, International Symposium on Identification and Determination of soil and rock parameters for geotechnical design., 2002.

[4] P. W. Mayne, Stress-strain-strength-flow parameters from enhanced in-situ tests. In Proc. Int. Conf. on In Situ Measurement of Soil Properties and Case Histories, Bali, 2001.

[5] S. E. Burns and P. W. Mayne , "Small-and high-strain measurements of in situ soil properties using the seismic cone penetrometer. Transportation Research Record, 1548(1), 81-88.," Transportation Research Record, vol. 1548, no. 1, pp. 81-88, 1996.

[6] S. Zhou, "Caracterisation des sols de surface a l'aide du penetrometre dynamique leger a energie variable type Panda," (Doctoral dissertation, Clermont-Ferrand 2), 1997.

[7] L. Chaigneau, "Caractérisation des milieux granulaires de surface à l'aide d'un pénétromètre," (Doctoral dissertation, Université Blaise Pascal, Clermont-Ferrand 2), 2001.

[8] B. O. Hardin and V. P. Drnevich, "Shear modulus and damping in soils: Measurement and parameter effects," vol. 98, pp. 603-624, 1972.

[9] H. Seed and I. Idriss, Soil moduli and damping factors for dynamic response analyses, Technical Report, University of California, Berkeley, California, 1970.

[10] J. Biarez and P. Y. Hicher, "Elementary mechanics of soil behaviour," Rotterdam, Netherlands: Balkema, 1994, 208p, 1994.

[11] M. Omidvar, D. Malioche Jeanne, S. Bless and M. Iskander, “Phenomenology of rapid projectile penetration into granular soils,” International Journal of Impact Engineering, vol. 85, pp. 146-160, 2015.
[12] M. Arlery, M. Gardou, J. M. Fleureau and C. Mariotti, “Dynamic behaviour of dry and water-saturated sand under planar shock conditions,” International Journal of Impact Engineering, vol. 37, no. 1, pp. 1-10, 2010.
[13] G. Aussedat, Sollicitations rapides des sols, Université de Grenoble: Doctoral dissertation, Ph. D. thesis, 1970.
[14] X. Cao, J. Chen, Y. Yu and Q. Wu, “An equation of state for abnormal expansion of shocked porous materials,” vol. 124, no. 21, 2018.
[15] S. P. Marsh, “LASL Shock Hugoniot Data,” University of California Press, 1980.
[16] M. Omidvar, M. Iskander and S. Bless, “Stress-strain behavior of sand at high strain rates,” vol. 49, pp. 192-213, 2012.
[17] M. A. Benz-Navarrete, Mesures dynamiques lors du battage du pénétromètre Panda 2, Université Blaise Pascal, Clermont II, 2009.
[18] E. Escobar, Mise au point et exploitation d’une nouvelle technique pour la reconnaissance des sols: le PANDA 3, University Blaise Pascal, Clermont II, 2015.
[19] R. Othman, “Comparison of three methods to separate waves in the processing of long-time Hopkinson bar experiments” vol. 5, pp. 114-119, 2014.
[20] M. N. Bussac, P. Collet, G. Gary and R. Othman, “An optimisation method for separating and rebuilding one-dimensional dispersive waves from multi-point measurements. Application to elastic or viscoelastic bars,” vol. 50, p. 32.
[21] H. Zhao and G. Gary, “A new method for the separation of waves. Application to the SHPB technique for an unlimited duration of measurement,” vol. 45, pp. 1185-1202, 1997.
[22] J. Carlsson, G. Sundin and B. Lundberg, “A method for determination of in-hole dynamic force-penetration data from two-point strain measurement on a percussive drill rod,” vol. 27, no. 6, pp. 553-558, 1990.
[23] E. Escobar, M. A. Benz-Navarrete, R. Gourvès, P. Breul and B. Chevalier, “In-situ determination of soil deformation modulus and the wave velocity parameters using the Panda 3®,” in Geotechnical and Geophysical Site Characterisation 5. Australian Geomechanics Society, Sydney, Australia, 2016.
[24] M. Emerson and P. Foray, “Laboratory P-wave measurements in dry and saturated sand,” Acta Geotechnica, vol. 1, no. 3, pp. 167-177, 2006.
[25] M. Aris, N. Benahmed and S. Bonelli, “Experimental geomechanics: a laboratory study on the behaviour of granular material using bender elements.,” 2012.
[26] A. Duttine, Comportement des sables et des mélanges sable/argile sous sollicitations statiques et dynamiques avec et sans « rotations d’axes », 2005.
[27] M. Emerson, Corrélations entre données géotechniques et géophysiques à faible profondeur dans des sables, 2005.
[28] R. Salgado, J. K. Mitchell and M. Jamiolkowski, Cavity expansion and penetration resistance in sand. Journal of Geotechnical and Geoenvironmental Engineering, 123(4), 344-354., 1997.